Physicochemical properties of concentrated Martian surface waters

Nicholas J. Tosca,[1] Scott M. McLennan,[2] Michael P. Lamb,[3] and John P. Grotzinger[3]

Received 27 July 2010; revised 1 December 2010; accepted 23 February 2011; published 17 May 2011.

[1] Understanding the processes controlling chemical sedimentation is an important step in deciphering paleoclimatic conditions from the rock records preserved on both Earth and Mars. Clear evidence for subaqueous sedimentation at Meridiani Planum, widespread saline mineral deposits in the Valles Marineris region, and the possible role of saline waters in forming recent geomorphologic features all underscore the need to understand the physical properties of highly concentrated solutions on Mars in addition to, and as a function of, their distinct chemistry. Using thermodynamic models predicting saline mineral solubility, we generate likely brine compositions ranging from bicarbonate-dominated to sulfate-dominated and predict their saline mineralogy. For each brine composition, we then estimate a number of thermal, transport, and colligative properties using established models that have been developed for highly concentrated multicomponent electrolyte solutions. The available experimental data and theoretical models that allow estimation of these physicochemical properties encompass, for the most part, much of the anticipated variation in chemistry for likely Martian brines. These estimates allow significant progress in building a detailed analysis of physical sedimentation at the ancient Martian surface and allow more accurate predictions of thermal behavior and the diffusive transport of matter through chemically distinct solutions under comparatively nonstandard conditions.

Citation: Tosca, N. J., S. M. McLennan, M. P. Lamb, and J. P. Grotzinger (2011), Physicochemical properties of concentrated Martian surface waters, *J. Geophys. Res.*, *116*, E05004, doi:10.1029/2010JE003700.

1. Introduction

[2] The detection of expansive salt deposits on Mars has made clear the influence of saline water early in Martian history. Sediments deposited from saline waters on Mars record abundant chemical information of their parent waters, including pH, redox, water activity, and anion content [*Catling*, 1999; *Marion and Kargel*, 2008; *Squyres et al.*, 2004; *Tosca et al.*, 2008; *Tosca and McLennan*, 2006]. In addition, primary mineral salts exhibit rapid response to postdepositional modification (including groundwater diagenesis, compaction, lithification, thermal history and oxidation), which can constrain the characteristics of the latest processes to have affected specific localities before liquid water was largely removed from the surface and subsurface [*Hardie*, 1991; *McLennan et al.*, 2005; *Smoot and Lowenstein*, 1991]. Detailed analysis of the Martian surface by landed and orbital exploration has revealed a detailed sedimentary record that contains not only the chemical signatures of an evolving planetary surface, but also the physical processes interwoven with that chemistry [*Grotzinger et al.*, 2005; *Grotzinger et al.*, 2006; *Malin and Edgett*, 2000; *McLennan and Grotzinger*, 2008]. Considering both chemical and physical processes of sedimentation on the ancient Martian surface will paint a more complete picture of paleoclimates, enabling more detailed characterization of surface evolution and perhaps habitability through time. The capability to estimate the chemical properties of Martian brines has provided an important step in the quantitative evaluation of habitability in saline environments, as factors such as water activity (a_{H2O}) and pH are important factors in determining habitable chemistry [*Knoll et al.*, 2005; *Marion and Kargel*, 2008; *Tosca et al.*, 2008]. Estimating the physical properties of Martian brines, however, allows a quantitative interpretation of physical sedimentary features (i.e., aeolian and fluvial), thermal properties of the surface and subsurface, and the fundamental transport of matter. Linking these properties to various data returned from both orbital and landed exploration requires that they be evaluated as a function of chemistry and saline mineralogy.

[3] Here we evaluate a broad spectrum of likely chemical compositions of Martian brines and estimate their chemical and physical properties. We attempt to capture the likely geochemical variation that Martian brines could exhibit. Further, we associate each brine with its thermodynamically

[1]Department of Earth Sciences, University of Cambridge, Cambridge, UK.
[2]Department of Geosciences, State University of New York at Stony Brook, Stony Brook, New York, USA.
[3]Division of Geological and Planetary Sciences, California Institute of Technology, Pasadena, California, USA.

0148-0227/11/2010JE003700

Table 1. Initial Dilute Fluid Compositions Used to Derive Stage 1 Brines[a]

	Brine 1	Brine 2	Brine 3	Brine 4	Brine 5	Brine 6
HCO_3/SO_4	–	2.08	0.708	0.282	0.00	0.00
pH	5.12	4.81	4.49	4.08	4.59	3.41
φ	0.9969	0.9958	0.9952	0.9948	0.9946	0.9100
IS (mol/kg)	3.09E-03	3.60E-03	3.86E-03	4.03E-03	4.11E-03	4.67E-03
a_{H2O}	0.9993	0.9994	0.9994	0.9994	0.9994	1.0000
ρ (g/cm^3)	0.9972	0.9972	0.9972	0.9972	0.9972	0.9972
Na	2.50E-05	2.50E-05	2.50E-05	2.50E-05	2.50E-05	2.50E-05
K	1.00E-05	1.00E-05	1.00E-05	1.00E-05	1.00E-05	1.00E-05
Ca	1.65E-04	1.65E-04	1.65E-04	1.65E-04	1.65E-04	1.65E-04
Mg	4.97E-04	4.97E-04	4.97E-04	4.97E-04	4.97E-04	4.97E-04
Fe(II)	3.56E-04	3.56E-04	3.56E-04	3.56E-04	3.56E-04	3.56E-04
Cl	5.00E-06	5.00E-05	7.50E-05	9.00E-05	1.00E-04	1.20E-04
SO_4	0.00E+00	4.99E-04	7.48E-04	8.94E-04	9.98E-04	1.17E-03
HCO_3	2.07E-03	1.02E-03	5.00E-04	1.92E-04	0.00E+00	0.00E+00
HSO_4	0.00E+00	5.89E-07	1.80E-06	5.60E-06	1.90E-06	3.32E-05
CO_3	1.54E-08	3.78E-09	9.04E-10	1.34E-10	0.00E+00	0.00E+00
Eutectic (K)	259.65	237.65	237.15	237.15	190.65	174.15

[a]Compositions are in mol/kg.

predicted saline mineralogy, establishing clear ties to physicochemical properties. Finally, we discuss the application of these properties to problems related to a more complete paleoclimatic reconstruction of the Martian surface.

2. Chemical Compositions of Saline Water on Mars

2.1. Dilute Fluid Chemistry

[4] One of the most significant controls on the composition of dilute waters at the Martian surface and/or subsurface is chemical weathering of Martian basalt. A number of experimental and theoretical studies have attempted to constrain the nature of dilute solutions derived from basalt [*Baker et al.*, 2000; *Hurowitz et al.*, 2005; *King et al.*, 2004; *Tosca et al.*, 2004; *Zolotov and Mironenko*, 2007]. In general, previous work underscores the importance of distinct bulk composition and relative dissolution rates of rock-forming mafic minerals such as olivine, pyroxene and basaltic glass. These controls on chemical weathering generally yield fluids that are highly enriched in Mg, Fe, SiO_2 and Ca [*Hurowitz et al.*, 2005; *Tosca et al.*, 2004; *Zolotov and Mironenko*, 2007]. There are, of course, a number of processes that may modify chemistry aside from chemical weathering, but we limit our discussion to experimental and theoretical constraints on the chemical weathering of basalt and consider subsequent chemical fractionation by saline mineral precipitation. If we accept that the relative proportion of major cations is representative of general chemical weathering of an average basalt on Mars, then the major unknown variable in dilute fluid chemistry is anion content (e.g., SO_4^{2-}, HCO_3^-, Cl^-). Anion content and the extent of chemical dissolution both affect pH [*Tosca and McLennan*, 2006]. Thus, by varying the SO_4/HCO_3 content of Martian waters (which will be controlled in part by atmospheric chemistry) while maintaining constant cation proportions, a large spectrum of likely fluid compositions can be evaluated in a relatively simple chemical framework [*Tosca and McLennan*, 2006].

[5] Table 1 shows six compositions of dilute aqueous fluids derived from chemical weathering of synthetic basalt. Cation proportions, taken from *Tosca and McLennan* [2006] and *Tosca et al.* [2004], are assumed to be modified by mineral dissolution, while anion compositions are controlled by varying the ratio of HCO_3 to SO_4 in the fluid, and allowing pH to be adjusted by charge balance, while maintaining equilibrium with a 1 bar atmosphere. For simplicity, all Fe is assumed to initially be in the Fe^{2+} state. At this fixed cation composition, varying the bicarbonate to sulfate ratio between HCO_3 and SO_4-dominated end-members leads to pH values between 5.12 and 3.41, respectfully. For the compositions in Table 1, the pH systematically decreases as a function of increasing SO_4 and decreasing HCO_3, according to the relationship shown by *Tosca and McLennan* [2006], where, for the purposes of modeling and generating a continuous spectrum of possible solution compositions, the "titration" of aqueous SO_4 to a composition controlled by fixed pCO_2 influences both pH and HCO_3/SO_4.

2.2. Brine Generation

[6] To generate concentrated solutions from our initial dilute fluids listed in Table 1, we utilize two thermodynamic models allowing calculations at 25°C (Geochemist's workbench) and also at low temperature (FREZCHEM) [*Marion and Kargel*, 2008; *Tosca et al.*, 2008; *Tosca and McLennan*, 2006]. The thermodynamic models both employ the Pitzer ion interaction model for the calculation of activity coefficients, the osmotic coefficients and mineral solubility at high ionic strength. The models have been discussed in detail by *Marion and Kargel* [2008], *Tosca et al.* [2008], and *Tosca and McLennan* [2006]. Mineral solubility from evaporating waters has been shown in natural and laboratory settings to closely correspond with thermodynamically predicted mineral assemblages [*Harvie et al.*, 1984; *Hardie and Eugster*, 1980]. In other words, saline minerals normally precipitate once thermodynamic saturation is reached, leaving thermodynamic calculations as close approximations to natural behavior. However, it is worth noting

Table 2. Stage 1 Brine Compositions and Physical Properties[a]

	Brine 1(a)	Brine 2(a)	Brine 3	Brine 4(a)	Brine 5(a)	Brine 6(a)
HCO_3/SO_4	–	2.08	0.708	0.282	0.00	0.00
pH_f	6.86	5.59	4.19	4.02	1.37	−0.2
φ	0.9099	0.6485	1.0410	1.1863	1.2437	1.7626
IS (mol/kg)	0.1794	7.2803	12.5620	13.8330	13.6850	13.0740
a_{H2O}	0.9937	0.9543	0.8816	0.8525	0.8423	0.7350
ρ (g/cm^3)	1.0074	1.1934	1.2999	1.3056	1.3061	1.3247
η_{298} (mPa s)	0.8911	4.2160	15.2804	17.2060	16.6439	17.6663
η_{273} (mPa s)	1.7789	9.7807	40.3848	44.4396	42.5414	41.5753
P (Pa; 25°C)	3150.31	3024.9	2793.9	2701.2	2660.9	2178.5
σ (mN/m)	72.24	73.92	77.19	78.77	79.01	81.83
λ W/(m K)	0.6073	0.5790	0.5541	0.5470	0.5461	0.5110
κ (mS/cm)	13.71	69.71	42.1707	36.80	43.81	107.58
D_{H2O} (m^2/s)	2.30E-09	1.53E-10	5.51E-11	2.84E-11	3.65E-11	1.88E-10
D_{Mg} (m^2/s)	6.91E-10	3.95E-11	2.64E-11	1.39E-11	1.76E-11	7.84E-11
D_{SO4} (m^2/s)	–	6.09E-11	1.97E-11	1.00E-11	1.29E-11	6.82E-11
D_{Na} (m^2/s)	1.29E-09	9.91E-11	4.02E-11	2.09E-11	2.67E-11	1.27E-10
D_H (m^2/s)	8.56E-09	6.13E-10	2.79E-10	1.46E-10	1.86E-10	8.38E-10
C_p (J/(kg K))	4133.16	3251.31	2918.3554	2777.72	2851.97	3410.23
Na	0.1250	0.1288	0.12883	0.1444	0.1649	0.1743
K	0.0500	0.0515	0.0515	0.0578	0.0659	0.0697
Ca	0.0004	0.0071	0.00207	0.0014	0.0015	0.0028
Mg	0.0010	1.7800	2.5611	2.3485	2.3095	2.1936
Fe(II)	0.0000	0.0018	0.55851	1.0980	1.0984	0.9535
Cl	0.0250	0.2576	0.38649	0.5200	0.6594	0.8368
SO_4	0.0000	1.7331	3.0165	3.2870	3.1630	2.3340
HCO_3	0.1526	0.0344	0.0044	0.0042	0.0000	0.0000
HSO_4	0.0000	0.0000	0.0000	0.0003	0.1277	2.0851
CO_3	1.34E-04	0.0000	0.0000	0.0000	0.0000	0.0000

[a]All values are at 25°C unless otherwise noted. Compositions are in mol/kg.

that for some mineral classes, including the Fe sulfates (in particular ferric and mixed valence phases), mineral precipitation may not occur at saturation and so these minerals may not precipitate until significant supersaturation levels are reached [*Alpers and Nordstrom*, 1999; *Tosca and McLennan*, 2009]. In this evaluation, we attempt to avoid these complications by specifying that all Fe remains in the ferrous state from start to finish. This justification

Table 3. Stage 2 Brine Compositions and Physical Properties[a]

	Brine 1(b)	Brine 2(b)	Brine 3	Brine 4(b)	Brine 5(b)	Brine 6(b)
HCO_3/SO_4	–	2.08	–	0.282	0.00	0.00
pH_f	7.73	5.03	–	0.623	0.67	−2.077
φ	0.9650	1.5539	–	2.0972	1.6844	2.8187
IS (mol/kg)	6.3392	13.0030	–	17.1630	14.2300	14.2910
a_{H2O}	0.8031	0.7221	–	0.5550	0.6971	0.3625
ρ (g/cm^3)	1.1533	1.3041	–	1.3552	1.3044	1.1467
η_{298} (mPa s)	1.0939	9.1259	–	12.4238	6.8971	18.3505
η_{273} (mPa s)	1.8077	20.2716		29.1402	14.8262	40.6163
P (Pa; 25°C)	2543.5	2287.7	–	1765.3	2125.85	821.2
σ (mN/m)	80.918	83.401	–	89.985	83.037	89.352
λ W/(m K)	0.5854	0.5398	–	0.4870	0.5040	0.3670
κ (mS/cm)	368.18	191.28	–	47.39	122.25	582.80
D_{H2O} (m^2/s)	2.45E-09	3.11E-10	–	2.13E-11	1.82E-10	4.92E-10
D_{Mg} (m^2/s)	–	1.23E-10	–	1.07E-11	7.74E-11	1.80E-10
D_{SO4} (m^2/s)	–	1.18E-10	–	7.24E-12	6.59E-11	1.82E-10
D_{Na} (m^2/s)	1.33E-09	2.05E-10	–	1.57E-11	1.24E-10	3.08E-10
D_H (m^2/s)	8.41E-09	1.37E-09	–	1.13E-10	8.44E-10	2.00E-09
C_p (J/(kg K))	512.03	3419.84	–	2773.60	3002.15	3095.58
Na	1.0979	1.7365	–	0.7646	1.1179	0.7071
K	5.2135	0.7919	–	0.8429	0.4470	0.2388
Ca	0.0000	0.0000	–	0.0000	0.0000	0.0000
Mg	0.0000	2.8398	–	2.2188	1.7644	1.9052
Fe(II)	0.0000	0.0000	–	2.4336	1.5233	0.2600
Cl	4.3721	4.2681	–	7.5826	4.4701	3.4090
SO_4	0.0000	1.9552	–	1.5959	2.2348	0.7011
HCO_3	1.8836	0.0294	–	0.0000	0.0000	0.0000
HSO_4	0.0000	0.0000	–	0.1108	0.2598	6.6043
CO_3	2.79E-02	0.0000	–	0.0000	0.0000	0.0000

[a]All values are at 25°C unless otherwise noted. Compositions are in mol/kg.

Table 4. Saline Mineralogy From Evaporation and Freezing Simulations[a]

	Brine 1(a)	Brine 1(b)	Brine 2(a)	Brine 2(b)	Brine 3	Brine 4(a)	Brine 4(b)	Brine 5(a)	Brine 5(b)	Brine 6(a)	Brine 6(b)
Evaporation Simulation											
Siderite	34.97	33.82	52.98	36.17	35.13	21.40	0.52	–	–	–	–
Calcite	16.21	15.67	–	–	–	–	–	–	–	–	–
Magnesite	48.82	47.21	22.62	15.59	–	–	–	–	–	–	–
Gypsum	–	–	24.40	16.66	16.97	39.15	95.39	32.93	17.48	29.15	17.67
Melanterite	–	–	–	–	–	17.98	1.37	37.72	34.04	38.69	37.06
Epsomite	–	–	–	31.30	47.90	21.47	2.72	29.34	48.48	32.16	31.24
Bloedite	–	–	–	0.24	–	–	–	–	–	–	–
Kieserite	–	–	–	–	–	–	–	–	–	–	14.01
Halite	–	–	–	–	–	–	0.01	–	–	–	0.01
Picromerite	–	–	–	0.04	–	–	–	–	–	–	–
KCl	–	0.46	–	–	–	–	–	–	–	–	–
$NaHCO_3$	–	2.37	–	–	–	–	–	–	–	–	–
$KHCO_3$	–	0.47	–	–	–	–	–	–	–	–	–
Freezing Simulation											
Siderite	35.00	–	47.00	33.33	33.33	–	–	–	–	–	–
Calcite	16.21	0.33	–	–	–	–	–	–	–	–	–
Magnesite	48.79	2.26	19.73	–	–	–	–	–	–	–	–
Gypsum	–	–	21.46	21.87	21.87	21.14	0.42	21.06	1.05	17.30	–
Melanterite	–	–	–	4.10	4.10	37.96	27.59	37.88	–	36.45	20.22
$MgSO_4\ 12H_2O$	–	–	11.81	40.70	40.70	40.90	61.34	41.05	67.90	46.26	56.38
$NaHCO_3$	–	82.50	–	–	–	–	–	–	–	–	–
$KHCO_3$	–	14.92	–	–	–	–	–	–	–	–	–
KCl	–	–	–	–	–	–	6.06	–	4.51	–	–
$NaCl\ 2H_2O$	–	–	–	–	–	–	–	–	6.80	–	–
Mirabilite	–	–	–	–	–	–	4.60	–	2.37	–	1.66
$MgCl_2\ 12H_2O$	–	–	–	–	–	–	–	–	17.37	–	–
$KHSO_4$	–	–	–	–	–	–	–	–	–	–	15.03
$Na_3H(SO_4)^2$	–	–	–	–	–	–	–	–	–	–	6.71

[a]Note that simulations are not carried to absolute completion but in a maximum of two stages only.

has been considered in more detail by *Tosca and McLennan* [2006].

[7] Our evaporation simulations were run at 25°C using dilute compositions specified in Table 1 and the geochemical model described in previous publications [*Tosca and McLennan*, 2006; *Tosca et al.*, 2008]. All simulations were run by specifying fractional crystallization and suppressing the formation of dolomite (assumed because no dolomite has been observed to be associated with Martian evaporate deposits and its formation is known to be kinetically inhibited on Earth), while allowing pH to vary, but subject to charge balance constraints. The simulations were performed in two stages. First, compositions from Table 1 were evaporated until the numerical simulation did not converge. Nonconvergence results from failure to meet the set convergence criterion ($\varepsilon < 5 \times 10^{-11}$) after 1000 consecutive iterations using the Newton-Raphson method in solving the equilibrium state of the system [*Marion et al.*, 2008]. The resulting compositions and mineralogy are labeled as "stage 1" brines and are tabulated in Table 2. The resulting aqueous composition was entered into a new (stage 2) simulation on the basis of 1000 g of total solution, with chemical components present in negligible amounts from stage 1 omitted. Mineralogy and resulting aqueous composition are tabulated and referred to herein as "stage 2" brines (Table 3). Evaporation simulations were only performed for two stages until nonconvergence resulted, and so represents a somewhat incomplete mineralogical composition if brines were evaporated to total completion. For the calculation of eutectic temperatures, we followed an analogous procedure using the FREZCHEM model, version 11.2 [*Marion and Kargel*, 2008; *Marion et al.*, 2008]. Because simulations were only run in two stages, mineralogy listed in Table 4 does not represent the total mineralogy upon completion. This approach was taken in order to provide a means of generating highly concentrated brine solutions in a geochemically relevant context.

2.3. Brine Compositions and Saline Mineralogy

[8] The chemical composition, saline mineralogy and major chemical and physical properties of solution compositions 1–6 are listed in Tables 2–4. Together, the brines exhibit significant variation in almost all chemical and physical properties and are associated with variable saline mineralogy. In general, the chemical compositions of the brines, as well as the predicted saline mineralogy, closely correspond with the "chemical divide" framework outlined by *Tosca and McLennan* [2006]. The least acidic composition, the bicarbonate-dominated end-member (brine 1), begins with an initial pH of 5.12 and a final pH of 7.73 at the completion of stage 2 evaporation. The mineralogy, unsurprisingly, is dominated by carbonate minerals (siderite, calcite and magnesite) in stage 1 evaporation. Upon stage 2 evaporation, the total mineral assemblage includes minor amounts of sylvite and bicarbonate salts. Brine 2, with an initial pH of 4.81, stays roughly constant with a final pH at the termination of stage 2 evaporation of 5.03. The stage 1 saline assemblage is dominated by siderite and magnesite, but calcite is replaced by gypsum, which is controlled by a relatively small amount of sulfate at the outset of evaporation. Upon further evaporation, epsomite is precipitated in abundance, with trace amounts of bloedite and picromerite.

Brine 3 was completely evaporated in only one simulation, owing to a high degree of convergence and a relatively simple mineralogical composition upon evaporation. The resulting saline assemblage is composed primarily of siderite, epsomite and gypsum. The pH again stays roughly constant from initial to final values, at 4.49 and 4.19, respectively. With still increasing SO_4 (and decreasing HCO_3/SO_4), brine 4 began at an initial pH of 4.08, but ended at a pH of 0.623. This low pH results from a progressive buildup of H^+ concentration assuming now mineral precipitation reactions involving H^+. But with the precipitation of solid-phase acid salts the pH will increase as H^+ is sequestered in solid form. The stage 1 saline assemblage is dominated by siderite, gypsum, melanterite and epsomite. At stage 2, the mineralogical composition is dominated by gypsum precipitation, with minor amounts of epsomite, melanterite and siderite. Brine 5 decreases to a final pH of 0.67 from an initial value of 4.59. The initial pH of 4.59 in brine 5 is slightly higher than the initial value in brine 4 because we remove the effects of equilibration with a CO_2 atmosphere. Over the entire pH range of this simulation, aside from slight variations in pH, the mineral assemblage is unchanged if CO_2 is removed, but model convergence is more difficult to achieve if it is included. The mineral assemblage is composed in both stages of gypsum, melanterite and epsomite. Brine 6, containing the most SO_4 and no HCO_3 is consequently the most acidic, decreasing to a pH (unscaled) of −2.077 from an initial value of 3.41. The assemblage is dominated by gypsum, melanterite and epsomite at the completion of stage 1, with the additional precipitation of kieserite and halite at the completion of stage 2. The appearance of kieserite is a function of significantly decreased water activity (a_{H2O}), whereby kieserite is stable at highly concentrated levels of Mg and SO_4.

[9] The saline mineralogy outlined in Table 4 is only representative of a limited number of brine compositions derived from basaltic weathering processes under the influence of a CO_2-dominated atmosphere and the input of SO_4 and Cl. Nevertheless, the general trends in saline mineralogy can be used as a guide to the chemical systems which they represent; carbonate-dominated, sulfate-dominated, or "intermediate" chemistry. Further discussion of how the chemistry and mineralogy listed in Tables 1–4 can be correlated to data from the Martian surface is provided below.

3. Physicochemical Properties of Martian Brines

3.1. Water Activity, Osmotic Coefficient, and Ionic Strength

[10] The water activity, osmotic coefficient and ionic strength are related in the sense that they reflect salinity and concentration levels of the bulk solution and the resultant effect on the solvent water [*Anderson and Crerar*, 1993; *Pitzer*, 1991]. Each of these three chemical properties is calculated with the same thermodynamic model that predicts mineral solubility in concentrated brines (discussed above). Importantly, because each of these properties reflects, directly or indirectly, the properties of the solvent, they are related to a number of physical properties which are dependent on the properties of the solvent. Thus, accurate calculation of these parameters lays the framework for estimating several physical properties from chemical composition (discussed in more detail below). Using the Pitzer ion interaction approach, the osmotic coefficient takes the form

$$(\phi-1)=\left(\frac{2}{\sum_i m_i}\right)\left[\frac{-A_\phi I^{3/2}}{(1+bI^{1/2})}\right]+\sum_c\sum_a m_c m_a\left(B^\phi_{ca}+ZC_{ca}\right)+\sum_c\sum_{c'} m_c m_{c'}\left(\Phi^\phi_{cc'}+\sum_a m_a\psi_{cc'a}\right)+\sum_a\sum_{a'} m_a m_{a'}\left(\Phi^\phi_{aa'}+\sum_c m_c\psi_{caa'}\right)\ldots \quad (1)$$

where m_c and m_a are molalities of cations and anions, respectively, A_ϕ is the Debye-Hückel parameter, I is ionic strength (where $I = 0.5\Sigma m_i z^2_i$), and B^ϕ_{ca}, C_{ca}, $\Phi^\phi_{ii'}$ $\psi_{ii'}$ are ionic strength-dependent virial coefficients, Z is a function of ion molality and charge, and the remaining terms are adjustable parameters or constants [*Pitzer*, 1991]. The osmotic coefficient reflects the summation of binary cation-anion interactions as well as triplet interactions between cations and anions. Together, the osmotic coefficient, related to the water activity (a_{H2O}), reflects the total nonideal behavior of thermodynamic quantities induced by elevated solute concentration:

$$a_{H_2O}=\exp\left(\frac{-\phi\sum_i m_i}{55.50844}\right) \quad (2)$$

The water activity, osmotic coefficient and ionic strength values are tabulated for stage 1 and stage 2 brine compositions in Tables 1–3. As is evident from their formal definitions, the values are useful measures of the degree of concentration and salinity of each brine. The accuracy and precision of calculating the osmotic coefficient and, hence, water activities of concentrated electrolyte solutions has been detailed in a number of studies aimed at deriving Pitzer ion interaction parameters (such as those required for equation (1)) for multicomponent systems [*Clegg et al.*, 1994; *Marion and Kargel*, 2008; *Pitzer*, 1991]. For example, the recalculation of experimentally measured osmotic coefficients and water activities from isopiestic data and vapor pressure measurements typically lies in the range of 1% or less [*Rard and Platford*, 1991; *Tosca et al.*, 2007]. The recalculation of mineral solubility data and solution compositions at saturation is on the order of only a few percent error [*Marion and Farren*, 1999; *Marion et al.*, 2008; *Pabalan and Pitzer*, 1991].

3.2. Solution Density

[11] The density of an aqueous solution can be estimated within the framework of the Pitzer ion interaction model, by summation of ion interaction effects on the volumetric properties of the solution [*Monnin*, 1990; *Pitzer*, 1991]. The volumetric properties of each brine listed in Table 1 are calculated using the FREZCHEM model, with details regarding density and volumetric properties at high ionic strength outlined by *Marion and Kargel* [2008]. The density of a given solution is calculated through the Pitzer

Table 5. Transformation of Brine Compositions to Solute Mixtures and Residuals (in mol/kg)

	Brine 1	Brine 2	Brine 3	Brine 4	Brine 5	Brine 6
			Stage 1			
$NaHCO_3$	0.1250	–	–	–	–	–
$KHCO_3$	0.0277	0.0344	–	–	–	–
KCl	0.0223	0.0171	–	0.0578	0.0659	0.0697
$MgCl_2$	0.0010	0.0469	–	–	–	–
NaCl	–	0.1288	–	0.1444	0.1649	0.1743
$MgSO_4$	–	1.7331	–	2.3485	2.3095	2.1936
$FeSO_4$	–	–	–	0.9385	0.9812	0.9535
$FeCl_2$	–	–	–	0.1595	0.1172	–
HCl	–	–	–	–	0.1942	0.5928
H_2SO_4	–	–	–	–	–	1.2720
Residuals						
Na	0.0000	0.0000		0.0000	0.0000	0.0000
K	0.0000	0.0000		0.0000	0.0000	0.0000
Ca	0.0004	0.0071		0.0014	0.0015	0.0028
Mg	0.0000	0.0000		0.0000	0.0000	0.0000
Fe(II)	0.0000	0.0018		0.0000	0.0000	0.0000
Cl	0.0007	0.0179		0.0012	0.0000	0.0000
SO_4T	0.0000	0.0000		0.0003	0.0000	0.0000
HCO_3	0.0001	0.0000		0.0042	0.0000	0.0000
			Stage 2			
$NaHCO_3$	–	–	–	–	–	–
$KHCO_3$	1.9393	–	–	–	–	–
KCl	3.2742	0.7919	0.0515	0.8429	0.4470	0.2388
$MgCl_2$	–	0.8846	0.1031	2.2188	1.4526	1.2316
NaCl	1.0979	1.7365	0.1288	0.7646	1.1179	0.7071
$MgSO_4$	–	1.9552	2.4580	–	0.3118	0.6736
$FeSO_4$	–	–	0.5585	1.7067	1.5233	0.2600
$FeCl_2$	–	–	–	0.7269	–	–
HCl	–	0.0295	–	0.0837	–	–
H_2SO_4	–	–	–	–	0.6595	6.3718
Residuals						
Na	0.0000	0.0000	0.0000	0.0000	0.0000	0.0000
K	0.0000	0.0000	0.0000	0.0000	0.0000	0.0000
Ca	0.0000	0.0000	0.0021	0.0000	0.0000	0.0000
Mg	0.0000	0.0000	0.0000	0.0000	0.0000	0.0000
Fe(II)	0.0000	0.0000	0.0000	0.0000	0.0000	0.0000
Cl	0.0000	0.0000	0.0000	0.0000	0.0000	0.0001
SO_4T	0.0000	0.0000	0.0000	0.0000	0.0001	0.0000
HCO_3	0.0278	0.0294	0.0044	0.0000	0.0000	0.0000

approach with knowledge of the volumetric properties of ionic species:

$$\rho = \frac{1000 + \sum_i m_i M_i}{\frac{1000}{\rho^o} + \sum m_i \overline{V_i}^o + V^{ex}} \tag{3}$$

where M_i is the molecular weight of species i, ρ_o is the density of pure water at a given temperature and pressure, $V^o{}_i$ is the partial molal volume at infinite dilution and V^{ex} is the excess volume of mixing, given by

$$\frac{V^{ex}}{RT} = f^v + 2\sum_c \sum_a m_c m_a \left[B^v_{ca} + \left(\sum_{cc'} m_c z_c \right) C^v_{ca} \right] \tag{4}$$

In equation (4), f^v, $B^v{}_{ca}$ and $C^v{}_{ca}$ are ionic strength-dependent functions containing adjustable parameters, z is the charge, R is the gas constant, and T is temperature in K [*Monnin*, 1990; *Pitzer*, 1991]. Volumetric parameters and partial molal volumes are given by *Monnin* [1990] and *Marion and Kargel* [2008] in addition to further derivation of the above equations. The standard deviation associated with recalculation of volumetric properties as well as solution densities of major sulfate and chloride chemistries of major cations and anions listed in Tables 1–3 is within the range of 10–500 × 10^{-6} cm^3/g [*Marion and Kargel*, 2008; *Monnin*, 1990].

3.3. Reconstitution of Brine Compositions as Solute Mixtures

[12] The methods discussed below for calculating physical properties are valid for highly concentrated multicomponent solutions. However, most of the methods require knowledge of single solute systems (e.g., NaCl-H_2O) as a function of concentration. These values are then used in mixing laws for multiple solute systems (e.g., NaCl-$MgSO_4$-H_2O) to calculate the property of the bulk solution. In most cases, the single solute properties are calculated at the same ionic strength or total molar concentration as the multicomponent mixture [*Miller*, 1996]. This complicates the determination of single solute data, because experimental data frequently only cover solution concentrations up to the limit of saturation with respect to a solid phase. This complication is introduced in the calculation of electrical conductivity and diffusion constants, discussed in more detail below. In an effort to circumvent this problem, there are theoretical methods available for calculation of single solute properties at high (i.e., supersaturated conditions) based on various analytical theories, and we employ these methods to generate realistic estimates of conductivity and diffusion coefficients [*Dufrêche et al.*, 2005]. This complication aside, none of the methods for physical property calculation, however, specify *how* the transformation from single ion concentrations (e.g., Na^+, Cl^-, Mg^{2+}, SO_4^{2-}) to solute mixtures (e.g., NaCl + $MgSO_4$) should be performed. Thus, we choose the transformation that best satisfies mass balance constraints of the total solution composition. Table 5 lists the brine compositions from Tables 2 and 3 in terms of mixtures of major solutes. Residual values between the single ion compositions in Tables 2 and 3, and the equivalent solute compositions are listed in Table 5. In all cases, the residual mass balance is negligible.

3.4. Dynamic Viscosity

[13] Our calculations of dynamic viscosity are performed using a generalized mixing rule derived by *Laliberté* [2007] for multicomponent electrolyte solutions, based on the measurement of viscosity for one-solute systems. The mixing rule is valid for up to 6 solutes dissolved in water, which requires recasting our solution compositions in terms of solute systems where charge and mass balance constraints are satisfied. This transformation, whether stage 1 or stage 2, also equates to six or less individual solutes with, in many cases, 4 solutes composing the majority of total dissolved solids. The mixing rule presented by *Laliberté* [2007] includes all of the solutes listed in Table 5. The general mixing equation used to derive the viscosity of a multicomponent electrolyte solution is

$$\ln \eta_m = w_w \ln \eta_w + \sum_i w_i \ln \eta_i \tag{5}$$

where w_w is the mass fraction of water, η_w is the viscosity of pure water at a specific temperature, and w_i is the mass

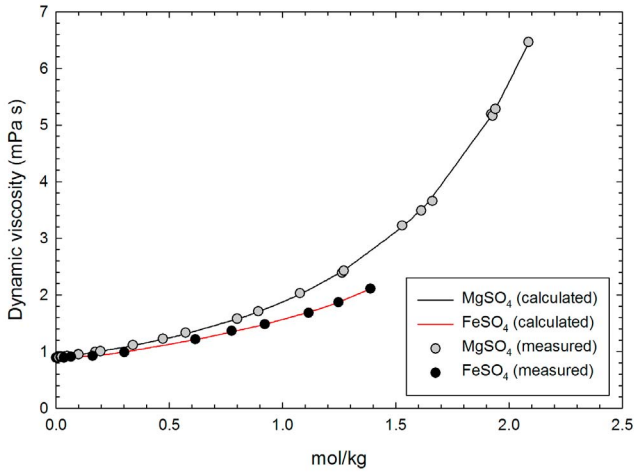

Figure 1. Comparison of calculated and measured dynamic viscosity of the $MgSO_4$-H_2O and $FeSO_4$-H_2O systems at 25°C as a function of concentration using the model developed by *Laliberté* [2007]. Experimental data are from *Laliberté* [2007].

fraction of solute i, subject to the constraint that for n solutes,

$$w_w + \sum_{i=1}^{n} w_i = 1 \tag{6}$$

The expression for the viscosity for pure water is

$$\eta_w = \frac{t + 246}{(0.05594T + 5.2842)t + 137.37} \tag{7}$$

where t is in °C and η_w is the viscosity in units of mPa s. An analysis and compilation of viscosity data over a range of temperature and concentration showed that the experimental viscosity data for solute i can be adequately represented with the following expression [*Laliberté*, 2007]:

$$\eta_i = \exp\left(\frac{v_1\ (1 - w_w)^{v_2} + v_3}{(v_4 + 1)(v_5(1 - w_w)^{v_6} + 1)}\right) \tag{8}$$

where v_1 to v_6 are dimensionless constants derived for each solute [*Laliberté*, 2007]. Available experimental data allow us to represent our brine compositions listed in Table 1 within the limits of concentration and temperature, with the substitution of Na_2CO_3 and K_2CO_3 for the $NaHCO_3$ and $KHCO_3$ components, respectively, because they do not approach the concentration levels reached for brines 1(a) and 1(b) (based on a comparison between viscosities of these components, they are reasonable substitutes). Recalculation of experimentally measured viscosity values is generally within 1% or less for the major solute systems listed in Table 5. As an example, the calculated and measured viscosities for $MgSO_4$, $FeSO_4$, H_2SO_4 and $MgCl_2$ are shown in Figures 1 and 2.

3.5. Eutectic Temperatures

[14] The eutectic temperatures (Table 1) calculated for the solution compositions given in Tables 2 and 3 were obtained using the FREZCHEM program [*Marion and Kargel*, 2008], which calculates chemical properties and mineral solubility of concentrated electrolyte solutions at low temperature, simulating the freezing process. For each calculation, we allowed the brine composition to continuously freeze, precipitating ice and a variety of saline minerals (assemblages corresponding to the freezing of 2 stage simulations only, are listed in Table 4). We specified open system behavior with respect to CO_2 and fractional crystallization. We continued the process with residual brine compositions until the eutectic composition was reached at a given temperature value. More details on the FREZCHEM program and its development are given by *Marion and Kargel* [2008].

3.6. Vapor Pressure

[15] The vapor pressure of H_2O(g) in equilibrium with a given aqueous solution can simply be related to its fugacity through the activity of water:

$$a_{H_2O} = \frac{f_{H_2O}}{f^o_{H_2O}} \tag{9}$$

where f^o_{H2O} is the fugacity of pure water at the same temperature as the solution and both solution and solvent are at a reference state pressure equal to the vapor pressure of pure water [*Rard and Platford*, 1991]. In calculating vapor pressure from fugacity, however, the nonideal behavior of water vapor must be accounted for. For this calculation, we use calculated osmotic coefficient values and their relation to the solution vapor pressure at equilibrium by

$$\phi = -\frac{\left(m_s / \sum_i v_i m_i\right)}{RT} \cdot \left\{RT \ln\left(\frac{P_s}{P^o_s}\right) + B_2(T)\left(P_s - P^o_s\right) + V^o_{s(l)}\left(P^o_s - P_s\right)\right\} \tag{10}$$

where P_s and P^o_s are the vapor pressure of the solvent and of pure water at standard state, respectively, and $V^o_{s(l)}$ is the

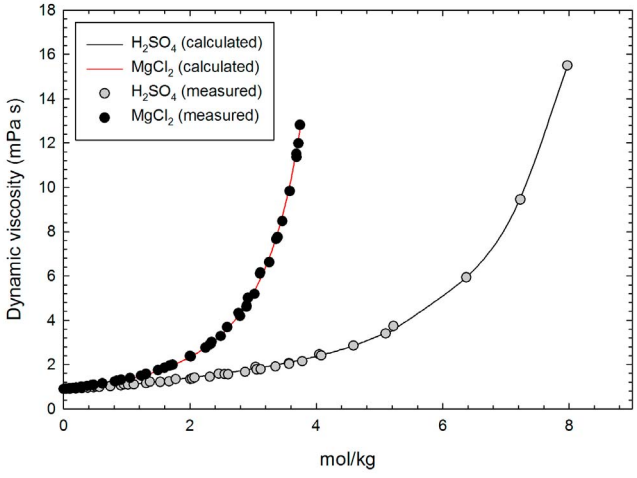

Figure 2. Comparison of calculated and measured dynamic viscosity of H_2SO_4-H_2O and $MgCl_2$-H_2O systems at 25°C as a function of concentration using the model developed by *Laliberté* [2007]. Experimental data are from *Laliberté* [2007].

molar volume of pure water at standard state. The saturation vapor pressure of pure water as a function of temperature has been compiled by *Rard and Platford* [1991] and is equal to 3168.62 Pa at 25°C. The $B_2(T)$ term has been calculated over a range of temperatures and is accurately represented with an empirical expression

$$B_2T = \frac{27.02}{(1+10^{-4}T)} - \frac{13193}{T} - 16.9704(1-\exp(-1500/T))^{\frac{5}{2}} \cdot \exp(1500/T)\left(\frac{T}{1500}\right)^{\frac{1}{2}} \quad (11)$$

where T is temperature in K and at 298.15 K yields -1157 cm^3/mol. This relationship is fundamentally derived from thermodynamics, and so error propagation in vapor pressure will largely stem from inaccuracies in the calculation of the osmotic coefficient, which, as discussed below, is less than 1% for the multicomponent electrolyte systems of interest. Utilizing this relationship allows experimentally determined vapor pressures to be used to derive osmotic coefficients (i.e., isopiestic experiments). The relationships described above, however, assume that the molar volume of pure water is approximately equal to the molar volume water in the electrolyte solution. This approximation introduces negligible error into the calculation of vapor pressure, because, as *Rard and Platford* [1991] point out, these two values rarely differ by more than 1 or 2 cm^3/mol.

3.7. Surface Tension

[16] The surface tension of an aqueous electrolyte solution is related to the concentration and type of ions present and is also strongly controlled by the osmotic coefficient, or water activity [*Hu and Lee*, 2004; *Li et al.*, 1999]. *Li et al.* [1999] derived a thermodynamic model to predict the surface tension of multicomponent electrolyte solutions based on experimental data for one solute systems. The model specifies that the surface tension of the solution is related to the chemical properties of the "surface phase" (S) of the solution, which is the interface between the vapor phase and the bulk solution phase (B). The surface phase is of constant concentration but its chemical properties are different than the bulk phase. Treating experimental surface tension data within this framework requires no specification of a surface phase thickness, but simply the inclusion of an empirical "interface parameter," g, that relates the chemical properties of the surface phase to the bulk phase. The relationship, assuming the osmotic coefficient is the same in the bulk and surface phases, is as follows:

$$\sigma_{solu} = \sigma_w + \frac{RT}{55.51A_w}\left(\phi^B \sum_i \nu_i m_i^B - \phi^S \sum_i g_i \nu_i m_i^B\right) \quad (12)$$

where T is temperature in K, σ_w is the surface tension of pure water at temperature (72 mN/m at 25°C), ν_i is the number of ions resulting from the dissociation of one molecule of electrolyte i, and A_w is the molar surface area of pure water:

$$A_w = \overline{A}_w = (V_w)^{2/3}(N_A)^{1/3} \quad (13)$$

where $\overline{A}_w$ is the partial molar surface area of water, V_w is the molar volume of pure water and N_A is Avagadro's number. When $g = 0$, as is the case for several one solute systems of relevance to the Martian surface (e.g., $MgSO_4$), equation (12) reduces to

$$\sigma_{solu} = \sigma_w - \frac{RT}{A_w}\ln a^B_{H_2O} \quad (14)$$

The model presented above for the recalculation of experimentally derived surface tension data generally results in <1–4 relative % agreement over a range of temperature and concentration for both single solute systems and mixed solvent multicomponent systems. For our system, experimental data have been tabulated and validated for HCl, NaCl, KCl, H_2SO_4, $MgCl_2$, and $MgSO_4$ [*Li et al.*, 1999]. For $FeSO_4$ and $FeCl_2$, we use the g values from $MgSO_4$ and $MgCl_2$, respectively. However, for the bicarbonate salts, we use 0 values of g, which provides reasonable estimates in the absence of experimental data [*Li et al.*, 1999], but these should be considered provisional until they can be verified experimentally.

3.8. Thermal Conductivity

[17] There have been a number of different approaches employed to accurately estimate the thermal conductivity of multicomponent electrolyte solutions [*Horvath*, 1985; *Riedel*, 1951; *Wang and Anderko*, 2008]. Among the simplest and most widely used approaches is that proposed by *Riedel* [1951], which provides good agreement with experimental data for a variety of electrolyte solutions (within 5%). A mixing rule was originally derived for a number of electrolyte systems at 20°C where the thermal conductivity of the electrolyte solution, λ_{solu}, is equal to

$$\lambda_{solu} = \lambda_{H_2O} + \sum_i a_i c_i \quad (15)$$

where λ_{H2O} is the thermal conductivity of pure water, c_i is the concentration of the ion, i (in mol/L, which requires conversion from molalities reported in Table 5 using density values), and a_i is a coefficient derived for each individual ion. This general mixing rule has been modified to accommodate mixed solvent systems and to obtain a higher degree of accuracy [*Horvath*, 1985], but the general form and the coefficients in equation (15) are still widely used. Unfortunately, this form of the mixing model is only valid to moderately concentrated electrolyte solutions and becomes less accurate in dealing with strong acids [*Horvath*, 1985; *Riedel*, 1951]. However, based on an extensive compilation of thermal conductivity data of single solute systems (including all of the solutes and the concentration ranges listed in Table 5), *Zaytsev and Aseyev* [1992] derived mixing parameters and coefficients valid for the calculation of thermal conductivity of mixed electrolyte systems at high concentration. The equation is only a slightly varied form of equation (15):

$$\lambda = \lambda_o\left[1 - \sum\nolimits_i \beta_i c_i\right] \quad (16)$$

where λ is the thermal conductivity of the solution in W/(m K), λ_o is the thermal conductivity of pure water in W/(m K), β_i

Table 6. Parameters for Thermal Conductivity Estimation

	Minimum (mol/kg)	Maximum (mol/kg)	$\beta_i \times 10^3$
$MgSO_4$	0.1662	1.8278	216.8
$FeSO_4$	0.1317	1.4483	226.4
HCl	0.5486	9.6001	331.2
H_2SO_4	0.5098	9.6866	489.9
$NaHCO_3$	0.2381	1.4285	172.3
$KHCO_3$	0.1998	2.5969	13.4
KCl	0.2683	3.2193	104.9
$MgCl_2$	0.2101	3.5711	477.9
NaCl	0.3422	4.2779	153.6
$FeCl_2$	0.1578	1.9724	290.0

are coefficients determined by mathematical processing of single solute data and c_i is the mass of the substance (in kg) per 1 kg of solution. The thermal conductivity of pure water is approximated with the polynomial:

$$\lambda_o = 0.5545 + 0.00246T - 0.00001184T^2 \tag{17}$$

where T is the temperature in °C. The coefficients for equation (16) and their concentration limits, determined by *Zaytsev and Aseyev* [1992], are listed in Table 6.

3.9. Electrical Conductivity

[18] Electrical conductivity is perhaps one of the most complicated physical properties to calculate for the brine compositions listed in Tables 1–3. The most recent and comprehensive treatment of electrical conductivity for concentrated multicomponent electrolyte solutions is detailed in a study by *Anderko and Lencka* [1997]. The approach uses the mean spherical approximation (MSA), which is an analytical theory capable of yielding accurate estimates of thermodynamic and transport properties for electrolyte solutions [*Anderko and Lencka*, 1997; *Bernard et al.*, 1992; *Dufrêche et al.*, 2005]. The MSA theory is analogous to the Debye-Huckel theory in that it can accommodate multicomponent solutions at moderately high concentrations. In essence, the MSA theory includes a more realistic method of including ion size effects into the Debye-Huckel theory; charges, diameters and concentrations of the ions are input into the calculations and the properties are expressed in terms of a dimensionless parameter, Γ [*Anderko and Lencka*, 1997; *Bernard et al.*, 1992; *Dufrêche et al.*, 2005]. The MSA theory allows accurate estimates of a number of physical properties of electrolyte solutions, including diffusion coefficients, which are discussed in detail below [*Anderko and Lencka*, 1998]. The treatment by *Anderko and Lencka* [1997] however, extends the MSA theory of single electrolyte solutions to very high concentrations by invoking the "effective ionic radius," which is an empirical representation of the ionic radius as a function of concentration. The parameters that define the effective ionic radius are derived from fitting experimental conductivity data to high concentration [*Anderko and Lencka*, 1997; *Huang and Papangelakis*, 2006]. For multicomponent solutions, the authors derived a mixing rule that expresses the specific conductivity of the electrolyte solution at a given concentration in terms of the concentration-dependent conductivities of the constituent ions:

$$\kappa = \sum_k^{N_T} c_k |z_k| \lambda_k \tag{18}$$

where N_T is the total number of ions and λ_k is the conductivity of the kth ion in a multicomponent solution. If experimental data at high concentration are lacking, the conductivity of a cation i in the presence of an anion j can be approximated from the mean spherical approximation (MSA) theory by obtaining an average value:

$$\lambda_k \cong \overline{\lambda_k} \tag{19}$$

where $\overline{\lambda_k}$ is obtained by averaging over all anions that exist in the mixture:

$$\overline{\lambda_i} = \sum_j^{N_A} f_j \lambda_{i(j)}(I) \tag{20}$$

where N_A is the total number of anions and $\lambda_{i(j)}$ is the conductivity of cation i in the presence of anion j, calculated at the ionic strength of the multicomponent mixture. Conversely, the conductivity of anion j in the presence of other cations in the mixture is calculated by

$$\overline{\lambda_j} = \sum_i^{N_C} f_i \lambda_{j(i)}(I) \tag{21}$$

where f_i, the equivalent fraction, is given by

$$f_i = \frac{|z_i| c_i}{c_{eq}} \tag{22}$$

where z_i is the charge and c_{eq}, the equivalent concentration, is defined as

$$c_{eq} = \sum_i^{N_C} c_i |z_i| = \sum_j^{N_A} c_j |z_j| \tag{23}$$

and

$$c_i = \frac{2I}{|z_i|(|z_i| + |z_j|)}; \quad c_j = \frac{2I}{|z_j|(|z_i| + |z_j|)} \tag{24}$$

Using the model described above, the representation of experimentally derived electrical conductivity data for single, double, and mixed solvent systems shows excellent agreement; generally within average deviations (expressed as AAD [*Anderko and Lencka*, 1997]) within 0.2–2.9%. However, application of this method to our solutions involves a number of pitfalls. For example, experimental conductivity data for single solutes are largely limited to ionic strengths below the total ionic strength present in some of our solutions (because they are bounded by saturation). To circumvent this problem, we used the MSA theory to approximate the electrical conductivity values of single-solute systems at these ionic strength levels and introduced the values into the mixing laws described above. The conductivity of an ion at finite concentration can be calculated by

$$\lambda_i = \lambda_i^0 \left(1 + \frac{\delta \nu_i^{el}}{\nu_i^0}\right)\left(1 + \frac{\delta X}{X}\right) \tag{25}$$

where λ_i^0 is the limiting conductivity of a given ion at infinite dilution, $\delta X/X$ is the relaxation effect and $\delta \nu_i^{el}/\nu^0{}_i$ is the electrophoretic correction [*Anderko and Lencka*, 1997;

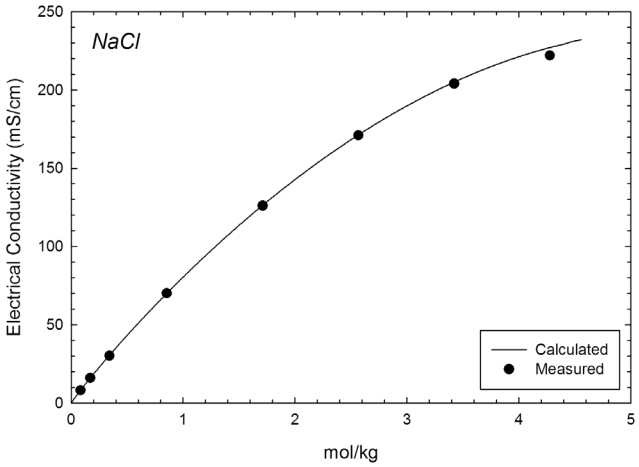

Figure 3. Comparison of calculated and measured electrical conductivity for NaCl-H_2O system at 25°C using the model developed by *Anderko and Lencka* [1997]. Experimental data are from *Lide* [1998].

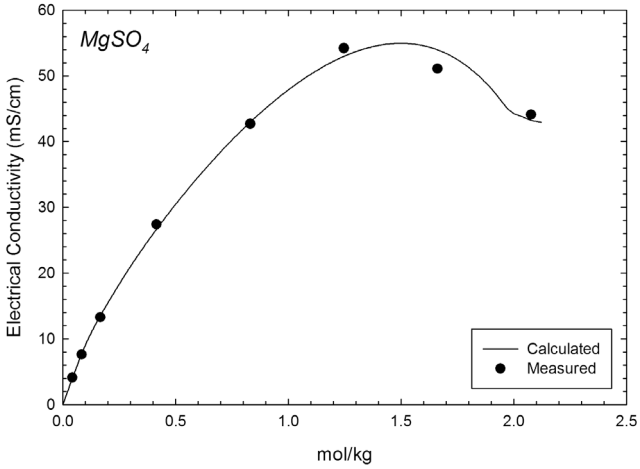

Figure 5. Comparison of calculated and measured electrical conductivity for $MgSO_4$-H_2O system at 25°C using a model developed by *Anderko and Lencka* [1997]. Experimental data are from *Lide* [1998].

Bernard et al., 1992]. The latter two terms are calculated with the MSA theory. The advantage of this approach, however, is that estimating the concentration dependence of conductivity for a given binary electrolyte solution requires only the limiting conductivities of the cation and anion, ionic diameters, ionic charges and the dielectric constant and viscosity of the solvent as a function of temperature (calculated above) [*Anderko and Lencka*, 1997; *Bernard et al.*, 1992]. Ionic diameters are difficult to calculate, but *Anderko and Lencka* [1997] have shown that crystallographic radii provide suitable approximations. We use crystallographic radii [from *Shannon and Prewitt*, 1969, 1970] for all systems except for the $MgSO_4$ system, for which previous workers have estimated the "effective" ionic diameters based on empirical analyses [*Huang and Papangelakis*, 2006], and for the NaCl, KCl, $MgCl_2$, HCl systems, for which parameters for the effective ion diameters were determined by *Anderko and Lencka* [1997]. The necessary equations for the relaxation effect and the electrophoretic correction, and their derivation are listed by *Anderko and Lencka* [1997], *Bernard et al.* [1992], and *Dufrêche et al.* [2005] and are not repeated here. It is important to note that to simplify our calculations, we follow *Sanchez-Castro and Blum* [1989] by approximating the 2Γ value in order to avoid a somewhat complicated nonlinear equation and also neglect the calculation of the $\delta X^{rel}_i/X$ term in the calculation of the relaxation effect, which is negligible even at very high concentrations [*Bernard et al.*, 1992]. Figures 3–5 compare our estimates of conductivity for binary electrolyte solutions (following the procedure described above) to experimental electrical conductivity data for the NaCl and $MgCl_2$ systems, as examples illustrating 1:1 and 1:2 electrolyte behavior with this model. Agreement is excellent for the NaCl system up to 4.13 mol/kg, but calculated values begin to deviate from experimental values for the $MgCl_2$ system at concentrations above 1 mol/kg. Nevertheless, the estimated behavior is well approximated for both systems and serves as a useful estimate to apply to the mixing rule (equation (18)) for our solution concentrations in Table 5. On the other hand, using the "effective" ionic diameters derived for the $MgSO_4$ system by *Huang and Papangelakis* [2006], the results are in excellent agreement, as shown in Figure 5. For the $FeSO_4$ and $FeCl_2$ systems, we substitute $MgSO_4$ and $FeSO_4$ values, respectively, at the same concentration levels, as compilations of conductivity for these systems show almost identical behavior [*Zaytsev and Aseyev*, 1992]. For the other binary systems, at worst, the results show similar deviation to the $MgCl_2$ system at high concentration. Nevertheless, our estimates are realistic and based on theory despite the paucity of experimental conductivity data at high concentration.

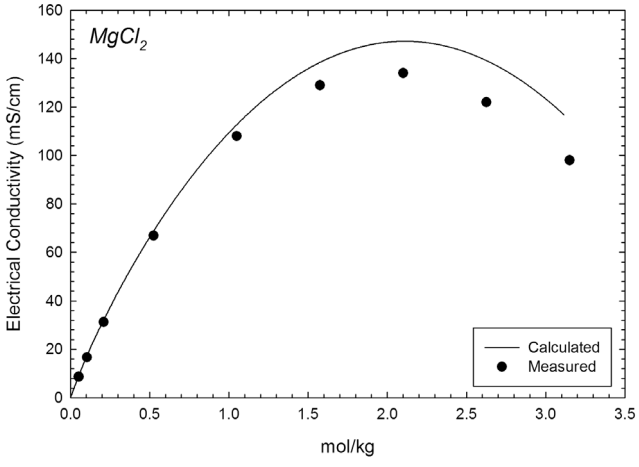

Figure 4. Comparison of calculated and measured electrical conductivity for $MgCl_2$-H_2O system at 25°C using the model developed by *Anderko and Lencka* [1997]. Experimental data are from *Lide* [1998].

3.10. Diffusion Coefficients

[19] A similar model incorporating the MSA theory in calculating diffusion coefficients of highly concentrated electrolyte solutions was presented by *Anderko and Lencka* [1998]. In short, a mixing model was proposed for multi-

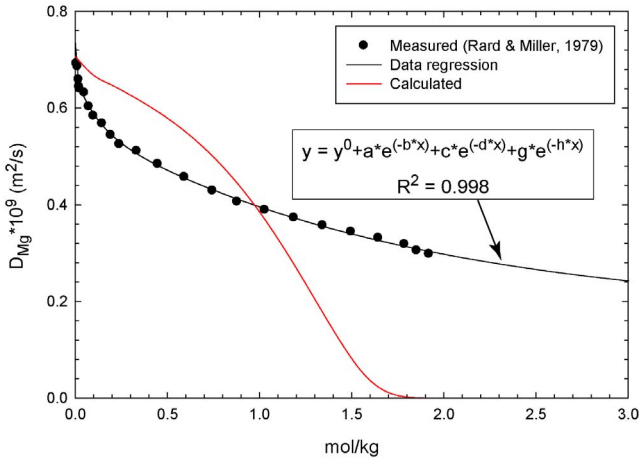

Figure 6. Comparison of calculated and measured diffusion coefficients for Mg^{2+} in the $MgSO_4$-H_2O system at 25°C as a function of concentration using a modified model developed by *Anderko and Lencka* [1998]. Experimental data are from *Rard and Miller* [1979]. The experimental data are fit well with a linearized exponential function but are in poor agreement with calculated values using the modified (with no provision for neutral species) model explained in the text.

component systems utilizing the Stefan-Maxwell equations for relating the fluxes of a species to chemical potential gradients in solution. In addition, the model allows the calculation of diffusion coefficients of single solute systems by specifying the concentration dependence of D_i by

$$D_i = D_i^o\left(1 + \frac{\delta k_i}{k_i}\right) \tag{26}$$

where D_i^o is the infinite dilution diffusion coefficient, which can be derived from the limiting diffusivities by the Nernst-Einstein equation [*Lasaga*, 1998; *Robinson and Stokes*, 2002], and $\delta k_i/k_i$ is the relaxation effect, calculated from MSA theory [*Bernard et al.*, 1992; *Dufrêche et al.*, 2005]. This relationship is accurate to moderately concentrated solutions up to ~1 mol/kg [*Anderko and Lencka*, 1998]. For even higher concentration levels, an additional parameter based on hard sphere theory is incorporated to the concentration dependence of the diffusion coefficient of single solute systems. However, to simplify our calculations, in cases where we calculated diffusion coefficients for single electrolytes at the same total number density as in the multicomponent mixture (as discussed below), we use only the relationship in equation (26). An important component of this model is the replacement of the average ion diameter with the effective ion diameter, which can be adjusted empirically to fit experimental data and appears in the calculation of the relaxation effect (equation (26)). Parameters for the calculation of the effective diameter were obtained for the single solute systems NaCl and $MgCl_2$ [*Anderko and Lencka*, 1998]. Similar to the electrical conductivity model, where parameters describing the effective ion diameter are lacking, crystallographic radii may be used [*Anderko and Lencka*, 1998]. In addition to the MSA-based approach for calculating diffusion coefficients, a tabulation and empirical regression of experimental diffusion coefficient values for single solute systems as a function of concentration for all of our solutes (except $NaHCO_3$ and $KHCO_3$) was presented by *Lobo* [1993]. These data supplement a previous compilation by *Zaytsev and Aseyev* [1992], and provide a means of comparing, and a supplementary means of estimating, diffusion coefficients at high concentration. With diffusion coefficients of single solute systems estimated, the mixing rule for calculating the diffusion coefficient of a major species in a multicomponent electrolyte solution is

$$D_i = \frac{n_T}{\sum_{d=1}^{N_c N_a} \frac{n_{s(d)} + n_{+(d)} + n_{-(d)}}{D_{i(d)}} + \sum_{l=1}^{N_n} \frac{n_{s(l)} + n_l}{D_{i(l)}}} \tag{27}$$

where n_T is the total number of moles of all components, $n_{s(d)}$ is the number of moles of solvent in a solution that contains the same total number of moles of solute d, $n_{s(l)}$ is the number of moles of solvent containing neutral species l, and $n_{+(d)}$ and $n_{-(d)}$ are the number of moles of the cation and anion that contain the solute d. In equation (27), $D_{i(d)}$ is the diffusion coefficient of species i in a single-solute system. If this value is unavailable from the literature, it can be calculated where

$$D_{i(d)} = \frac{n_{s(d)} + n_{+(d)} + n_{-(d)}}{\frac{n_{s(d)}}{a_{is}} + \frac{n_{+(d)}}{a_{i+}} + \frac{n_{-(d)}}{a_{i-}}} \tag{28}$$

$$D_{i(l)} = \frac{n_{s(l)} + n_l}{\frac{n_{s(l)}}{a_{is}} + \frac{n_l}{a_{il}}} \tag{29}$$

In the above equations, the interaction coefficients, a_{ij}, are calculated with the Stefan-Maxwell equations, which is valid for electrolytes up to ~4 mol/kg [*Pinto and Graham*, 1986] and require the knowledge of ion mobility (calculated through Stokes law [*Pinto and Graham*, 1986; *Robinson and Stokes*, 2002]), viscosity (discussed above), and the electrophoretic effect (calculated by MSA theory). It is worth noting, however, that the interaction coefficients are largely independent of concentration and the type of species present in the system [*Anderko and Lencka*, 1998; *Pinto and Graham*, 1986]. Estimating the contribution of neutral species in a highly concentrated electrolyte solution is problematic because accurate speciation models under these conditions are not known. The effects of neutral species are anticipated to be the most important for divalent metal sulfate solutions. Figure 6 illustrates this point; we include no effects of neutral $MgSO_4^0$ species which are known to be important in this system at elevated concentration [*Rard and Clegg*, 1999]. As an alternative, a linearized exponential function can be fit to experimental $MgSO_4$ data beyond 0.4 molal ($R^2 = 0.9947$) to simulate a gradual decrease in the diffusion coefficient with concentration. This approach is probably more realistic because it is a conservative extrapolation of experimentally determined values. Aside from divalent metal sulfate systems, estimations of diffusion coefficients for other single electrolyte systems are in good agreement with experimental data even when the neutral complexes are neglected (Figure 7 and 8) and thus are suitable estimates to incorporate into the mixing rule in equations (27)–(29).

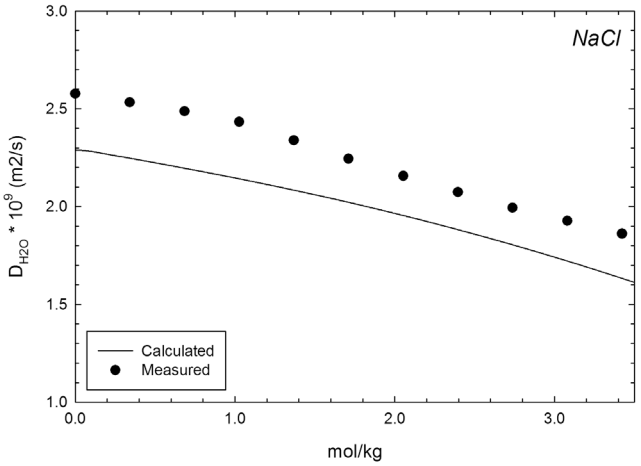

Figure 7. Comparison of calculated and measured diffusion coefficients for H_2O in the NaCl-H_2O system at 25°C using a modified model developed by *Anderko and Lencka* [1998]. Experimental data are from *Zaytsev and Aseyev* [1992].

3.11. Heat Capacity

[20] The heat capacity of a given electrolyte solution can be estimated within the framework of the Pitzer ion interaction model [*Pitzer*, 1991], but a simpler and sufficiently accurate method based on a double polynomial expression was used by *Zaytsev and Aseyev* [1992]. The utility of the model depends on the available experimental heat capacity data for single solute systems, and so the model was applied to the compilation of heat capacity data reported by *Zaytsev and Aseyev* [1992]. For our electrolyte solutions, each component is represented with this model, and the experimental data on which the model is based cover the range of concentrations listed in Table 5. The heat capacity of a multicomponent electrolyte solution can be estimated by the double polynomial:

$$C_p = C_{p,w} + \sum_i \left(B_{1i} + B_{2i}c_i^{'} + B_{3i}T + B_{4i}T^2\right)c^i \qquad (30)$$

where T is temperature in °C, $C_{p,w}$ is the heat capacity of pure water (J/(kg K)) and can be calculated to within 0.01% by the following polynomial between 0 and 100°C:

$$C_{p,w} = 4217.591 - 371.6753\tau + 1436.422\tau^2 - 3043.413\tau^3 + 3819.384T^4 - 2538.933T^5 + 696.99867T^6 \qquad (31)$$

where $\tau = 0.01$, and

$$c_i^{'} \frac{1}{E_i} \sum_j E_j c_j \qquad (32)$$

where E_i and B_{1i} is a coefficient (listed in Table 7). This method of estimation reproduces the compiled experimentally measured thermal conductivity data of *Zaytsev and Aseyev* [1992] to within 2–3%.

4. Limitations

[21] The evaporation of basaltic weathering derived solutions results in distinct chemical compositions. For most of the physical properties discussed above (e.g., diffusion coefficients), our solution compositions involve the inclusion of data at concentrations beyond where experimental studies have investigated. In several cases, there is a strong theoretical framework that allows such values to be calculated at the required concentrations. Worse yet, in some circumstances, the physical property values for some components are merely substitutes, or approximations. However, in these cases, it is important to underscore that they are estimates only and must be validated with experimental data. For most properties (specifically viscosity, density, surface tension, thermal conductivity and heat capacity), enough experimental data exist to bracket our solution compositions and provide enough of a foundation where our calculations can be shown to be in good agreement with experimental determinations. Nevertheless, with several analytical theories and their performance summarized here, an important first step has been taken toward more accurate calculation of physicochemical properties of these unique brine compositions.

5. Applications

[22] Layered evaporitic sediments at Meridiani Planum record the influence of highly concentrated solutions in initially forming and subsequently altering saline minerals [*Grotzinger et al.*, 2005; *Squyres and Knoll*, 2005]. In addition, several distinct styles of cross stratification identified throughout the Burns Formation provide clear examples of both aeolian and subaqueous processes in sediment deposition at Meridiani. Collectively, the cross-stratified sediments record a dominantly aeolian depositional environment punctuated by periods where water was available at the surface. Of significant importance, however, is the identification of cross stratification at Meridiani Planum, in the form of meter-scale low-angle cross bedding, as well as centimeter-scale trough (or festoon geometry) cross lamination [*Grotzinger et al.*, 2005, 2006]. The distinction between these two cross-stratification styles (and their

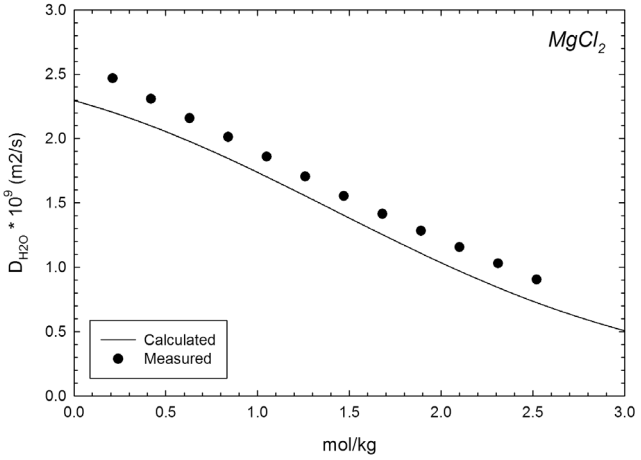

Figure 8. Comparison of calculated and measured diffusion coefficients for H_2O in the $MgCl_2$-H_2O system at 25°C using a modified model developed by *Anderko and Lencka* [1998]. Experimental data are from *Zaytsev and Aseyev* [1992].

Table 7. Parameters for Heat Capacity Estimation

	Minimum (mol/kg)	Maximum (mol/kg)	B_{1i}	B_{2i}	B_{3i}	$B_{4i} \times 10^3$	$E_i \times 10^2$
$MgSO_4$	0.1662	1.8278	−6029.6	6534.9	12.5	0	33.0
$FeSO_4$	0.1317	1.4483	−5311.4	2367.0	14.9	−12.0	151.4
HCl	0.5486	19.2002	−6701.2	0	21.6	0	194.0
H_2SO_4	0.5098	10.1964	−3826.9	1372.7	0	9.2	122.8
$NaHCO_3$	0.2381	1.4285	−2435.4	17889.5	5.3	0	–
$KHCO_3$	0.1998	2.1974	−3085.7	−13368.4	13.8	0	–
KCl	0.2683	3.2193	−5204.7	2021.7	2.1	−18.1	70.3
$MgCl_2$	0.2101	3.5711	−6304.3	3082.9	7.9	−13.9	129.7
NaCl	0.3422	4.1068	−5189.8	4869.9	5.2	−12.3	86.2
$FeCl_2$	0.1578	1.9724	−6200.0	3350.0	0	0	–

scales) allows a more complete environmental reconstruction at Meridiani Planum by unraveling the role of both eolian and fluvial processes in deposition and diagenesis [*Grotzinger et al.*, 2005; *McLennan and Grotzinger*, 2008]. More specifically, physical sedimentological analysis of bed form geometries and their scales can be used to quantify flow velocities and bed form stabilities under various depositional conditions [*Grotzinger et al.*, 2005; *Southard and Boguchwal*, 1990a, 1990b]. The most important variables that figure into the determination of flow velocity and bed form geometries include, among others, sediment density, fluid density and fluid viscosity [*Grotzinger et al.*, 2005; *Southard and Boguchwal*, 1990a 1990b]. These three variables can be assumed and, although their influence is minor, more quantitative estimates of these parameters and their relationship to chemistry and mineralogy provides a guide for more accurate reconstruction of depositional environments where concentrated aqueous solutions played a role.

[23] More specifically, physical sedimentological analysis of particle sizes and bed form types preserved in strata can be used to quantify the velocity and depth of flows responsible for transporting and depositing sediment on Mars [*Komar*, 1980; *Southard and Boguchwal*, 1990b; *Grotzinger et al.*, 2005]. Bed form stability fields are well described by a semiempirical framework of nondimensional parameters that depend on, among other things, the acceleration of gravity, sediment density, and kinematic viscosity ($\mu = \eta/\rho$) [*Southard and Boguchwal*, 1990a]. Application of this work to Mars has focused on the shift in bed form stability due to reduced gravity on Mars, which indicates that, for example, equivalent bed forms on Mars form from a flow with a velocity that is about three quarters that on Earth [*Southard and Boguchwal*, 1990b; *Grotzinger et al.*, 2005]. This, however, is probably a minor effect considering the potential for a 35-fold increase in viscosity of Martian brines compared to freshwater (e.g., $\mu = 3.56 \times 10^{-5}$ for brine 6(b); Table 2). *Boguchwal and Southard* [1990] showed that flow velocity reconstructed from bed forms compared to a reference case is changed by a factor of $(\mu/\mu_r)^{1/3}$, where μ_r is the kinematic viscosity for the reference case. This relationship was confirmed in hot water flume experiments where a two thirds reduction in effective flow velocity was found for a decrease in kinematic viscosity from 1.17×10^{-6} m^2/s to 3.69×10^{-7} m^2/s (corresponding to a water temperature change from 13°C to 77°C) [*Boguchwal and Southard*, 1990]. Although little work has been done to explore bed form stability under flows with viscosities significantly greater that that of pure water, *Grazer* [1982] used a water-sucrose solution with a kinematic viscosity of 1.05×10^{-5} m^2/s, which is about a factor of 10 greater than pure water at 25°C and approaches the upper estimate for Martian brines, and formed ripples consistent with the scaling analysis. This suggests that ripples and other bed forms developed by flowing Martian brines might form under flow conditions distinct from that of pure water with velocity scaling factors as high as 3.3 (i.e., $(\mu/\mu_r)^{1/3} = (3.5 \times 10^{-5}/1 \times 10^{-6})^{1/3} = 3.3$).

[24] Using density and viscosity estimates as a function of saline mineralogy not only applies to the Meridiani Planum case but is likely to provide an important framework for the interpretation of sedimentary features that could be encountered in future exploration missions, specifically the Mars Science Laboratory (MSL) mission. The candidate MSL landing sites include localities that, from orbital data, appear to contain layered sediments composed of phyllosilicates as well as sulfate minerals, with the most impressive example being Gale Crater, which contains ~5 km of layered sediments [*Thomson et al.*, 2008]. Quantitative estimates of densities and fluid viscosities as a function of mineralogy will provide an important framework for the interpretation of sedimentary features for such localities. The theoretical framework developed here is incorporated in a detailed companion study of bed form stability and physical sedimentology in concentrated surface waters on Mars (M. P. Lamb et al., Were aqueous ripples on Mars formed by brines?, submitted to *Journal of Sedimentary Research*, 2010). This companion study examines, in quantitative detail, the consequences of sediment and fluid density/viscosity estimated here for physical sedimentation on the ancient surface of Mars.

[25] The thermal properties of saline solutions estimated in this study will also provide a number of constraints on problems relating to the activity of saline water at the surface or subsurface, particularly in response to thermal processes that may occur as a function of obliquity. Specifically, thermal conductivity and heat capacity have a direct influence on controlling heat transfer through the subsurface. For example, *Kargel et al.* [2007] suggested that salt (or clathrate) hydrates have low thermal conductivity compared to typical basaltic bedrock and sediment and so this contrast would lead to thermal anomalies within the subsurface that would possibly sustain a saline hydrologic cycle. The study considered only solid phases, but our thermal conductivity of saline solutions shows that their thermal properties are of a similar order (Tables 2 and 3). In addition, problems related to thermal perturbations and heat conductance (e.g., heating, cooling, convection) can be approached using properties that are derived from the values

estimated here [*Lasaga*, 1998]. For example, the thermal diffusivity, which could be used to estimate times involved for thermal equilibration, is derived from density, thermal conductivity and heat capacity [*Lasaga*, 1998].

[26] In addition to subsurface thermal properties influenced by saline minerals or their parent solutions, recent surface processes will also be controlled in part by the thermal behavior of highly concentrated brines and the eutectics of saline assemblages, both of which we estimate above. For example, the recent formation of gullies on Mars is thought to have been induced by thermal perturbations and solar insolation [*Carr*, 2007; *Chevrier and Altheide*, 2008; *Schon et al.*, 2009]. As saline assemblages are exposed to temperatures above their eutectic, the first appearance of solution is, in most cases, saline [*Marion and Kargel*, 2008]. Thus, an understanding of the thermal properties and eutectic temperatures of these solutions may even be used in reverse to constrain mineralogy related to recent surface water flow on Mars if the temperature interval at the specific locality is constrained. Furthermore, the temporal stability of recent saline solutions at the surface of Mars is controlled by evaporation rates [*Chevrier and Altheide*, 2008]. Evaporation rates for the solutions listed in Tables 1–3 can be derived from the equilibrium vapor pressure and water activities of a given solution [*Chevrier and Altheide*, 2008; *Sears and Chittenden*, 2005; *Sears and Moore*, 2005]. This could provide constraints on the lifetime of such solutions at the surface of Mars and also serve as a theoretical basis for interpreting experimental evaporation rates. Vapor pressures in equilibrium with a given aqueous solution are also related to relative humidity which is important for stability relations of saline mineral hydrates and cycling of water at the Martian surface [*Vaniman et al.*, 2004].

[27] The diffusion coefficients and electrical conductivity have a number of applications to understanding saline geochemistry and mineralogy at the Martian surface. Specifically, the problem of concretion growth at Meridiani Planum has been treated with diffusion-based models [*McLennan et al.*, 2005; *Sefton-Nash and Catling*, 2008] and all of these require knowledge of diffusion coefficients for specific ions in highly concentrated solutions that are thought to have infiltrated evaporite bearing sediments [*McLennan et al.*, 2005; *Tosca et al.*, 2008]. Our estimates are directly applicable to these models; for example, solution 5 is the most consistent with observed saline mineralogy at Meridiani Planum [*Tosca and McLennan*, 2006]. Modeling diffusion processes is not limited to concretion growth, however. Molecular diffusion is a primary mechanism of the physical transport of matter through solids and liquids and modeling the kinetic problems that result from such transport mechanisms requires the knowledge of various diffusion coefficients [*Lasaga*, 1998]. For example, in low water-rock ratio environments where fluid flow is negligible, diffusion-limited processes dominate [*Berner*, 1978; *Lasaga*, 1998]. Thus, a number of important water-rock reactions, including primary mineral dissolution rates and secondary precipitation kinetics all require more quantitative knowledge of diffusion coefficients under such conditions. Our estimates provide a step toward quantification of these constants and the introduction of a simplified version of a well-established and flexible model to calculate diffusion in highly concentrated fluids can be improved upon with continued study.

[28] As our understanding of the geologic evolution of the Martian surface advances, there will be an increasing need for a quantitative framework with which to interpret geologic observations in a process-oriented manner. Although Mars has clearly followed a different evolutionary trajectory than the Earth, the same physical and chemical principles apply to the processes that shaped its surface. Asking how these processes change under relevant but nonstandard conditions will continue to spawn testable and informed hypotheses for planetary evolution.

[29] **Acknowledgments.** We thank John Southard for helpful discussions. N.J.T. is grateful for support from Churchill College, Cambridge.

References

Alpers, C. N., and D. K. Nordstrom (1999), Geochemical modeling of water-rock interactions in mining environments, in *The Environmental Geochemistry of Mineral Deposits. Part A: Processes, Techniques, and Health Issues*, edited by G. S. Plumlee and M. J. Logsdon, pp. 289–323, Soc. of Econ. Geol., Littleton, Colo.

Anderko, A., and M. M. Lencka (1997), Computation of electrical conductivity of multi-component aqueous systems in wide concentration and temperature ranges, *Ind. Eng. Chem. Res.*, *36*, 1932–1943, doi:10.1021/ie9605903.

Anderko, A., and M. M. Lencka (1998), Modeling self-diffusion in multi-component aqueous electrolyte systems in wide concentration ranges, *Ind. Eng. Chem. Res.*, *37*, 2878–2888, doi:10.1021/ie980001o.

Anderson, G. M., and D. A. Crerar (1993), *Thermodynamics in Geochemistry: The Equilibrium Model*, 588 pp., Oxford Univ. Press, New York.

Baker, L. L., D. J. Agenbroad, and S. A. Wood (2000), Experimental hydrothermal alteration of a Martian analog basalt: Implications for Martian meteorites, *Meteorit. Planet. Sci.*, *35*, 31–38, doi:10.1111/j.1945-5100.2000.tb01971.x.

Bernard, O., W. Kunz, P. Turq, and L. Blum (1992), Conductance in electrolyte solutions using the mean spherical approximation, *J. Phys. Chem.*, *96*, 3833–3840, doi:10.1021/j100188a049.

Berner, R. A. (1978), Rate control of mineral dissolution under earth surface conditions, *Am. J. Sci.*, *278*, 1235–1252, doi:10.2475/ajs.278.9.1235.

Boguchwal, L. A., and J. B. Southard (1990), Bed configurations in steady unidirectional water flows. Part 1. Scale model study using fine sands, *J. Sediment. Petrol.*, *60*(5), 649–657.

Carr, M. H. (2007), *The Surface of Mars*, 322 pp., Cambridge Univ. Press, Cambridge, U. K., doi:10.1017/CBO9780511536007.

Catling, D. C. (1999), A chemical model for evaporites on early Mars: Possible sedimentary tracers of the early climate and implications for exploration, *J. Geophys. Res.*, *104*, 16,453–16,469, doi:10.1029/1998JE001020.

Chevrier, V., and T. S. Altheide (2008), Low temperature aqueous ferric sulfate solutions on the surface of Mars, *Geophys. Res. Lett.*, *35*, L22101, doi:10.1029/2008GL035489.

Clegg, S. L., J. A. Rard, and K. S. Pitzer (1994), Thermodynamic properties of 0–6 mol kg^{-1} aqueous sulfuric acid from 273.15 to 328.15 K, *J. Chem. Soc. Faraday Trans.*, *90*, 1875–1894, doi:10.1039/ft9949001875.

Dufrêche, J.-F., O. Bernard, S. Durand-Vidal, and P. Turq (2005), Analytical theories of transport in concentrated electrolyte solutions from the MSA, *J. Phys. Chem. B*, *109*, 9873–9884, doi:10.1021/jp050387y.

Grazer, R. A. (1982), Experimental study of current ripples using medium silt, M.S. thesis, 131 p., Mass. Inst. of Technol., Cambridge.

Grotzinger, J. P., et al. (2005), Stratigraphy and sedimentology of a dry to wet eolian depositional system, Burns Formation, Meridiani Planum, Mars, *Earth Planet. Sci. Lett.*, *240*, 11–72, doi:10.1016/j.epsl.2005.09.039.

Grotzinger, J. P., et al. (2006), Sedimentary textures formed by aqueous processes, Erebus crater, Meridiani Planum, Mars, *Geology*, *34*, 1085–1088, doi:10.1130/G22985A.1.

Hardie, L. A. (1991), On the significance of evaporites, *Annu. Rev. Earth Planet. Sci.*, *19*, 131–168, doi:10.1146/annurev.ea.19.050191.001023.

Hardie, L. A., and H. P. Eugster (1980), Evaporation of seawater: Calculated mineral sequences, *Science*, *208*, 498–500, doi:10.1126/science.208.4443.498.

Harvie, C. E., N. Møllera, and J. H. Weare (1984), The prediction of mineral solubilities in natural waters: The Na-K-Mg-Ca-H-Cl-SO_4-OH-HCO_3-CO_3-CO_2-H_2O system to high ionic strengths at 25°C, *Geochim. Cosmochim. Acta*, *48*, 723–751, doi:10.1016/0016-7037(84)90098-X.

Horvath, A. L. (1985), Handbook of Aqueous Electrolyte Solutions: Physical Properties, Estimation and Correlation Methods, 631 pp., John Wiley, New York.

Hu, Y.-F., and H. Lee (2004), Prediction of the surface tension of mixed electrolyte solutions based on the equation of Patwardhan and Kumar and the fundamental Butler equations, *J. Colloid Interface Sci.*, *269*, 442–448, doi:10.1016/S0021-9797(03)00703-3.

Huang, M., and V. G. Papangelakis (2006), Electrical conductivity of concentrated $MgSO_4$-H_2SO_4 solutions up to 250°C, *Ind. Eng. Chem. Res.*, *45*, 4757–4763, doi:10.1021/ie0507631.

Hurowitz, J. A., S. M. McLennan, D. H. Lindsley, and M. A. A. Schoonen (2005), Experimental epithermal alteration of synthetic Los Angeles meteorite: Implications for the origin of Martian soils and identification of hydrothermal sites on Mars, *J. Geophys. Res.*, *110*, E07002, doi:10.1029/2004JE002391.

Kargel, J. S., R. Furfaro, O. Prieto-Ballesteros, J. A. P. Rodriguez, D. R. Montgomery, A. R. Gillespie, G. M. Marion, and S. E. Wood (2007), Martian hydrogeology sustained by thermally insulating gas and salt hydrates, *Geology*, *35*, 975–978, doi:10.1130/G23783A.1.

King, P. L., D. T. Lescinsky, and H. W. Nesbitt (2004), The composition and evolution of primordial solutions on Mars, with application to other planetary bodies, *Geochim. Cosmochim. Acta*, *68*, 4993–5008, doi:10.1016/j.gca.2004.05.036.

Knoll, A. H., et al. (2005), An astrobiological perspective on Meridiani Planum, *Earth Planet. Sci. Lett.*, *240*, 179–189, doi:10.1016/j.epsl.2005.09.045.

Komar, P. D. (1980), Modes of sediment transport in channelized water flows with ramifications to the erosion of the martian outflow channels, *Icarus*, *42*(3), 317–329, doi:10.1016/0019-1035(80)90097-4.

Laliberté, M. (2007), Model for calculating the viscosity of aqueous solutions, *J. Chem. Eng. Data*, *52*, 321–335, doi:10.1021/je0604075.

Lasaga, A. C. (1998), *Kinetic Theory in the Earth Sciences*, 811 pp., Princeton Univ. Press, Princeton, N. J.

Li, Z.-B., Y.-G. Li, and J.-F. Lu (1999), Surface tension model for concentrated electrolyte aqueous solutions by the Pitzer equations, *Ind. Eng. Chem. Res.*, *38*, 1133–1139, doi:10.1021/ie980465m.

Lide, D. R. (Ed.) (1998), *CRC Handbook of Chemistry and Physics*, 79th ed., CRC Press, Boca Raton, Fla.

Lobo, V. M. M. (1993), Mutual diffusion coefficients in aqueous electrolyte solutions, *Pure Appl. Chem.*, *65*, 2613–2640, doi:10.1351/pac199365122613.

Malin, M. C., and K. S. Edgett (2000), Sedimentary rocks of early Mars, *Science*, *290*, 1927–1937, doi:10.1126/science.290.5498.1927.

Marion, G. M., and R. E. Farren (1999), Mineral solubilities in the Na-K-Mg-Ca-Cl-SO_4-H_2O system: A re-evaluation of the sulfate chemistry in the Spencer-Moller-Weare model, *Geochim. Cosmochim. Acta*, *63*, 1305–1318, doi:10.1016/S0016-7037(99)00102-7.

Marion, G. M., and J. S. Kargel (2008), Cold Aqueous Planetary Geochemistry with FREZCHEM: From Modeling to the Search for Life at the Limits, 251 pp., Springer, Berlin.

Marion, G. M., J. S. Kargel, and D. C. Catling (2008), Modeling ferrous-ferric iron chemistry with application to Mars surface geochemistry, *Geochim. Cosmochim. Acta*, *72*, 242–266, doi:10.1016/j.gca.2007.10.012.

McLennan, S. M., and J. P. Grotzinger (2008), The sedimentary rock cycle of Mars, in *The Martian Surface: Composition, Mineralogy, and Physical Properties*, edited by J. F. Bell, pp. 541–577, Cambridge Univ. Press, Cambridge, U. K, doi:10.1017/CBO9780511536076.025.

McLennan, S. M., et al. (2005), Provenance and diagenesis of the evaporite-bearing Burns Formation, Meridiani Planum, Mars, *Earth Planet. Sci. Lett.*, *240*, 95–121, doi:10.1016/j.epsl.2005.09.041.

Miller, D. G. (1996), Approximations and relations between specific conductance, molar conductance, equivalent conductance and ionar conductance for mixtures, *J. Phys. Chem.*, *100*, 1220–1226, doi:10.1021/jp951157u.

Monnin, C. (1990), The influence of pressure on the activity-coefficients of the solutes and on the solubility of minerals in the system Na-Ca-Cl-SO_4-H_2O to 200°C and 1 kbar, and to high NaCl concentration, *Geochim. Cosmochim. Acta*, *54*, 3265–3282, doi:10.1016/0016-7037(90)90284-R.

Pabalan, R. T., and K. S. Pitzer (1991), Mineral solubilities in electrolyte solutions, in *Activity Coefficients in Electrolyte Solutions*, edited by K. S. Pitzer, pp. 435–490, CRC Press, Boca Raton, Fla.

Pinto, N. G., and E. E. Graham (1986), Evaluation of diffusivities in electrolyte solutions using Stefan-Maxwell equations, *AIChE J.*, *32*, 291–296, doi:10.1002/aic.690320216.

Pitzer, K. S. (1991), Ion interaction approach: Theory and data correlation, in *Activity Coefficients in Electrolyte Solutions*, edited by K. S. Pitzer, pp. 75–154, CRC Press, Boca Raton, Fla.

Rard, J. A., and S. L. Clegg (1999), Isopiestic determination of the osmotic coefficient and activity coefficients of $\{zH_2SO_4+(1-z)MgSO_4\}$ at T = 298.15 K. II. Results for z = (0.43040, 0.28758, and 0.14399) and analysis with Pitzer's model, *J. Chem. Thermodyn.*, *31*, 399–429, doi:10.1006/jcht.1998.0461.

Rard, J. A., and D. G. Miller (1979), The mutual diffusion coefficients of Na_2SO_4−H_2O and $MgSO_4$−H_2O at 25°C from Rayleigh interferometry, *J. Solution Chem.*, *8*, 755–766, doi:10.1007/BF00648779.

Rard, J. A., and R. F. Platford (1991), Experimental methods: Isopiestic, in *Activity Coefficients in Electrolyte Solutions*, edited by K. S. Pitzer, pp. 209–278, CRC Press, Boca Raton, Fla.

Riedel, L. (1951), Die Waermeleitfaehigkeit von waessrigen Loesungen starker Elektrolyte, *Chem. Ing. Tech.*, *23*, 59–64, doi:10.1002/cite.330230303.

Robinson, R. A., and R. H. Stokes (2002), *Electrolyte Solutions*, 571 pp., Dover, Mineola, N. Y.

Sanchez-Castro, C., and L. Blum (1989), Explicit approximation for the unrestricted mean spherical approximation for ionic solutions, *J. Phys. Chem.*, *93*, 7478–7482, doi:10.1021/j100358a043.

Schon, S. C., J. W. Head, and C. I. Fassett (2009), Unique chronostratigraphic marker in depositional fan stratigraphy on Mars: Evidence for ca. 1.25 Ma gully activity and surficial meltwater origin, *Geology*, *37*, 207–210, doi:10.1130/G25398A.1.

Sears, D. W. G., and J. D. Chittenden (2005), On laboratory simulation and the temperature dependence of the evaporation rate of brine on Mars, *Geophys. Res. Lett.*, *32*, L23203, doi:10.1029/2005GL024154.

Sears, D. W. G., and S. R. Moore (2005), On laboratory simulation and the evaporation rate of water on Mars, *Geophys. Res. Lett.*, *32*, L16202, doi:10.1029/2005GL023443.

Sefton-Nash, E., and D. C. Catling (2008), Hematitic concretions at Meridiani Planum, Mars: Their growth timescale and possible relationship with iron sulfates, *Earth Planet. Sci. Lett.*, *269*, 366–376, doi:10.1016/j.epsl.2008.02.009.

Shannon, R. D., and C. T. Prewitt (1969), Effective ionic radii in oxides and fluorides, *Acta Crystallogr., Sect. B Struct. Crystallogr. Cryst. Chem.*, *25*, 925–946, doi:10.1107/S0567740869003220.

Shannon, R. D., and C. T. Prewitt (1970), Revised values of effective ionic radii, *Acta Crystallogr., Sect. B Struct. Crystallogr. Cryst. Chem.*, *26*, 1046–1048, doi:10.1107/S0567740870003576.

Smoot, J. P., and T. K. Lowenstein (1991), Depositional environments of non-marine evaporites, in *Evaporites, Petroleum, and Mineral Resources*, edited by J. L. Melvin, pp. 189–347, Elsevier, Amsterdam, doi:10.1016/S0070-4571(08)70261-9.

Southard, J. B., and L. A. Boguchwal (1990a), Bed configurations in steady unidirectional flows. Part 2. Synthesis of flume data, *J. Sediment. Petrol.*, *60*, 658–679.

Southard, J. B., and L. A. Boguchwal (1990b), Bed configurations in steady unidirectional flows. Part 3. Effects of temperature and gravity, *J. Sediment. Petrol.*, *60*, 680–686.

Squyres, S. W., and A. H. Knoll (2005), Sedimentary rocks at Meridiani Planum: Origin, diagenesis, and implications for life on Mars, *Earth Planet. Sci. Lett.*, *240*, 1–10, doi:10.1016/j.epsl.2005.09.038.

Squyres, S. W., et al. (2004), In-situ evidence for an ancient aqueous environment at Meridiani Planum, Mars, *Science*, *306*, 1709–1714, doi:10.1126/science.1104559.

Thomson, B. J., N. T. Bridges, R. E. Milliken, J. F. Bell, W. M. Calvin, and C. M. Weitz (2008), New constraints on the origin and evolution of the layered deposits in Gale Crater, Mars, *Lunar Planet. Sci., XXXIX*, Abstract 1456.

Tosca, N. J., and S. M. McLennan (2006), Chemical divides and evaporite assemblages on Mars, *Earth Planet. Sci. Lett.*, *241*, 21–31, doi:10.1016/j.epsl.2005.10.021.

Tosca, N. J., and S. M. McLennan (2009), Experimental constraints on the evaporation of partially oxidized acid-sulfate waters at the Martian surface, *Geochim. Cosmochim. Acta*, *73*, 1205–1222, doi:10.1016/j.gca.2008.11.015.

Tosca, N. J., S. M. McLennan, D. H. Lindsley, and M. A. A. Schoonen (2004), Acid-sulfate weathering of synthetic Martian basalt: The acid fog model revisited, *J. Geophys. Res.*, *109*, E05003, doi:10.1029/2003JE002218.

Tosca, N. J., A. Smirnov, and S. M. McLennan (2007), Application of the Pitzer ion interaction model to isopiestic data for the $Fe_2(SO_4)_3$–H_2SO_4–H_2O system at 298.15 and 323.15 K, *Geochim. Cosmochim. Acta*, *71*, 2680–2698, doi:10.1016/j.gca.2007.03.020.

Tosca, N. J., A. H. Knoll, and S. M. McLennan (2008), Water activity (a_{H2O}) and the challenge for life on early Mars, *Science*, *320*, 1204–1207, doi:10.1126/science.1155432.

Vaniman, D. T., D. L. Bish, S. J. Chipera, C. I. Fialips, J. W. Carey, and W. C. Feldman (2004), Magnesium sulfate salts and the history of water on Mars, *Nature*, *431*, 663–665, doi:10.1038/nature02973.

Wang, P., and A. Anderko (2008), Modeling thermal conductivity of concentrated and mixed-solvent electrolyte systems, *Ind. Eng. Chem. Res.*, *47*, 5698–5709, doi:10.1021/ie071373c.

Zaytsev, I. D., and G. G. Aseyev (1992), *Properties of Aqueous Solutions of Electrolytes*, 1773 pp., CRC Press, Boca Raton, Fla.

Zolotov, M. Y., and M. V. Mironenko (2007), Timing of acid weathering on Mars: A kinetic-thermodynamic assessment, *J. Geophys. Res.*, *112*, E07006, doi:10.1029/2006JE002882.

J. P. Grotzinger and M. P. Lamb, Division of Geological and Planetary Sciences, California Institute of Technology, 1200 E. California Blvd., Pasadena, CA 91125, USA.

S. M. McLennan, Department of Geosciences, State University of New York at Stony Brook, 100 Nicolls Rd., Stony Brook, NY 11794, USA.

N. J. Tosca, Department of Earth Sciences, University of Cambridge, Downing Street, Cambridge CB2 3EQ, UK. (njt41@cam.ac.uk)